PROCEEDINGS OF SPIE

SPIEDigitalLibrary.org/conference-proceedings-of-spie

Optimisation of multimodal coherent anti-Stokes Raman scattering microscopy for the detection of isotope-labelled molecules

Dale Boorman, Iestyn Pope, Wolfgang Langbein, Steve Hood, Paola Borri, et al.

Dale Boorman, Iestyn Pope, Wolfgang Langbein, Steve Hood, Paola Borri, Peter Watson, "Optimisation of multimodal coherent anti-Stokes Raman scattering microscopy for the detection of isotope-labelled molecules," Proc. SPIE 10890, Label-free Biomedical Imaging and Sensing (LBIS) 2019, 1089005 (4 March 2019); doi: 10.1117/12.2509280

SPIE.

Event: SPIE BiOS, 2019, San Francisco, California, United States

Downloaded From: https://www.spiedigitallibrary.org/conference-proceedings-of-spie on 13 Mar 2019 Terms of Use: https://www.spiedigitallibrary.org/terms-of-use

Optimisation of multimodal coherent anti-Stokes Raman scattering microscopy for the detection of isotope-labelled molecules

Dale Boorman*[1], Iestyn Pope[1], Wolfgang Langbein[2], Steve Hood[3], Paola Borri[1] and Peter Watson[1]

[1]School of Biosciences, Sir Martin Evans building, Cardiff University, Museum Avenue, Cardiff, Wales, CF10 3AX, United Kingdom; [2]School of Physics and Astronomy, Cardiff University, The Parade, Cardiff, CF24 3AA, United Kingdom; [3]GSK Medicines Research Centre, Gunnels Wood Road, Stevenage, Hertfordshire, SG1 2NY, United Kingdom

ABSTRACT

Coherent anti-Stokes Raman scattering (CARS) microscopy utilises intrinsic vibrational resonances of molecules to drive inelastic scattering of light, and thus eradicates the need for exogenous fluorescent labelling, whilst providing high-resolution three-dimensional images with chemical specificity. Replacement of hydrogen atoms with deuterium presents a labelling strategy that introduces minimal change to compound structure yet is compatible with CARS due to an induced down-shift of the CH_2 peak into a region of the Raman spectrum which does not contain contributions from other chemical species, thus giving contrast against other cellular components.

We present our work using deuterated oleic acid to optimise setup of an in-house-developed multimodal, multiphoton, laser-scanning microscope for precise identification of carbon-deuterium-associated peaks within the silent region of the Raman spectrum. Application of the data analysis procedure, factorisation into susceptibilities and concentrations of chemical components (FSC^3), enables the identification and quantitative spatial resolution of specific deuterated chemical components within a hyperspectral CARS image. Full hyperspectral CARS datasets were acquired from HeLa cells incubated with either deuterated or non-deuterated oleic acid, and subsequent FSC^3 analysis enabled identification of the intracellular location of the exogenously applied deuterated lipid against the chemical background of the cell. Through application of FSC^3 analysis, deuterium-labelling may provide a powerful technique for imaging small molecules which are poorly suited to conventional fluorescence techniques.

Keywords: nonlinear optics, coherent anti-Stokes Raman scattering, hyperspectral image analysis, lipids, isotope labelling

1. INTRODUCTION

Whilst fluorescence microscopy remains the most widely used optical tool for imaging cellular components with high spatial resolution, with technologies such as super-resolution light microscopy achieving resolution in the submicrometre range, the technology is limited by a necessity for exogenous label incorporation to enable chemical specificity[1]. The majority of these fluorescent labels share a similar molecular weight with many small biological molecules, consequently affecting their physical and chemical properties[2-5]. Fluorophores are also susceptible to photobleaching with prolonged excitation and cells can become damaged by light at the necessary wavelengths, leading to difficulties in observing samples over longer timescales[6]. Phase contrast and differential interference contrast microscopy offer a label-free alternative to fluorescence microscopy which can provide high-resolution spatial images, but at the expense of chemical specificity[7]. Various analytical methods can be employed to obtain detailed information about chemical composition of cell extracts but fail to provide spatial information due to their invasive nature.

Label-free Biomedical Imaging and Sensing (LBIS) 2019, edited by Natan T. Shaked, Oliver Hayden, Proc. of SPIE Vol. 10890, 1089005 · © 2019 SPIE
CCC code: 1605-7422/19/$18 · doi: 10.1117/12.2509280

Downloaded From: https://www.spiedigitallibrary.org/conference-proceedings-of-spie on 13 Mar 2019
Terms of Use: https://www.spiedigitallibrary.org/terms-of-use

Spontaneous Raman microspectroscopy has emerged as a non-invasive, label-free optical technique which can be used to determine the chemical composition of endogenous components in cells based on intrinsic vibrational resonances of molecules which relate to the mass of the constitutive atoms and the strength of the chemical bonds between those atoms[8]. However, the technique is limited by a small cross-sectional area, thus necessitating a high excitation energy and long integration time to achieve a sufficient signal-to-noise ratio, which is not always compatible with living systems[9]. The scattered Raman field is also detected within the Stokes region, which overlaps with fluorescence emissions from endogenous molecules and can obscure the signal of interest. Coherent Raman scattering (CRS) techniques, such as coherent anti-Stokes Raman scattering (CARS), offer an alternative to spontaneous Raman scattering which can overcome the aforementioned limitations due to constructive interference of Raman scattered light from coherently driven molecular vibrations within the focal plane[10,11]. Two laser beams, a pump and a Stokes beam, with frequencies ω_p and ω_s, respectively, drive vibration in a material at the frequency difference, $\omega_p - \omega_s$. In CARS, the vibrational response is probed by the pump beam, resulting in coherent emission at $2\omega_p - \omega_s$, which is blue-shifted from the excitation frequency, thus permitting distinction of spectra from the endogenous background fluorescence. Unlike spontaneous Raman, all molecules within the focal volume are driven coherently and thus the emitted CARS intensity scales with the square of the number of identical molecular bonds.

Hyperspectral CARS is a progression of CARS technology which offers superior chemical specificity compared to single-frequency CARS through acquisition of spatially resolved images at a series of vibrational frequencies, thus producing a spectrum for every spatial point[12]. These spectra can be processed to retrieve Raman-like spectra which are linear in concentration of chemical components, thus overcoming the limitation of non-trivial line-shape which is associated with CARS due to interference between vibrationally resonant and non-resonant terms[13,14]. We have also recently described a data analysis algorithm, "Factorisation into Susceptibilities and Concentrations of Chemical Components" (FSC^3), which we employ with hyperspectral CARS data to provide unsupervised and unbiased quantitative chemical analysis of biological material in the form of spatially resolved images and retrieved chemical spectra[15]. With this system, we can produce quantitative chemical maps of independently varying chemical components within cells in their vol/vol concentrations.

The spectra of many chemical bonds overlap, thus making identification of a spectrum corresponding specifically to a particular chemical component challenging. For example, an abundance of vibrational resonances exists within the "CH-stretch" region of the CARS spectrum (2600-3400cm^{-1}) due to modes of methine (CH), methylene (CH_2), methyl (CH_3) and vinyl (=CH-) groups[16]. Consequently, the use of isotopologues as markers has emerged to provide improved contrast of a chemical of interest against the mixed chemical background of a cell[17]. Selective replacement of hydrogen with its neutron-containing heavier isotope, deuterium, presents a novel labelling strategy which induces minimal structural change to a molecule and is compatible with CARS imaging[18]. The larger molecular mass of the deuterium atom markedly shifts the vibrational frequency of the CARS signal into an otherwise silent region of the Raman spectrum between 1800cm^{-1} and 2700cm^{-1}, thus avoiding interference with other chemical species and providing contrast between the CARS signal from the deuterated molecule and that from the chemical background of the cell[18]. C-D-associated peaks have been identified between 2000cm^{-1} and 2500cm^{-1} for deuterated small molecules using spontaneous Raman scattering[19,20] although detection of the dissolved compounds from their solvent background lacked sensitivity. Deuterium labelling has also been used in conjunction with Raman-based imaging strategies to study cellular uptake and metabolism of fatty acids[21], cholestrol[22,23], glucose[24] and proteins[25,26], as well as their involvement in diseases such as atherosclerosis[27] and cancer[28].

We have previously shown the ability of our in-house CARS system and subsequent data analysis procedure for detecting small changes in lipid droplet composition[29,30,31]. Here, we use deuterated oleic acid to explore the ability of our in-house-built multimodal CARS microscope to identify and spatially resolve a chemical component representing a deuterated molecule with subcellular resolution and absolute concentration. Through acquisition of hyperspectral CARS images and subsequent FSC^3 analysis, we can identify an exogenously applied, deuterium-labelled molecule within a cell, which offers potential for studying molecule distribution, accumulation and metabolism. Hyperspectral CARS images of cytosolic lipid droplets were acquired from HeLa cells fed with deuterated and non-deuterated oleic acid, and

Downloaded From: https://www.spiedigitallibrary.org/conference-proceedings-of-spie on 13 Mar 2019
Terms of Use: https://www.spiedigitallibrary.org/terms-of-use

unsupervised FSC[3] analysis was performed to produce concentration maps of chemical components, thus enabling direct comparison of the chemical composition of lipid droplets.

2. MATERIALS & METHODS

2.1 Lipids

Bulk pure (>95%) oleic acid (OA), a monounsaturated 18C molecule with a cis double bond at the ninth carbon, and D17-oleic acid (D17-OA), with 17 deuterium atoms attached to carbons 11-18, were purchased from Cayman Chemical (MI, USA). The chemical structures of both deuterated and non-deuterated isoforms of oleic acid are shown in Table 1.

Table 1. Chemical structures of deuterium-labelled and unlabelled isoforms of oleic acid.

Oleic Acid	D17-Oleic Acid
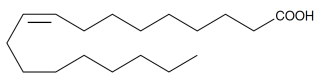	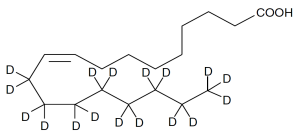

2.2 Cell culture and treatment

Human cervical carcinoma (HeLa) cells (ATCC, UK) were cultured in minimum essential medium (MEM) supplemented with GlutaMAX™ (Life Technologies, UK) and 10% (v/v) foetal bovine serum (FBS) (Life Technologies, UK). Cells were grown directly on glass coverslips (thickness #1.5, 25mm diameter, PA, VWR International, USA). Following 8 hours incubation in MEM + GlutaMAX™ with 10% FBS, cells were transferred to MEM + GlutaMAX™ supplemented with lipid-free FBS (Biowest, France) to deplete cells of lipid droplets. Following an 18-hour incubation period, cells were transferred to MEM + GlutaMAX™ supplemented with lipid-free FBS and a complex of bovine serum albumin (BSA) (Sigma Aldrich, UK) and the investigated fatty acid (47 µg/ml fatty acid concentration). Fatty acid-BSA complexes were formed by adapting a published protocol[32]. Following a further 18-hour incubation period, coverslips were fixed in a 4% formaldehyde-PBS solution (Affymetrix, UK) for 20 minutes and mounted onto standard glass microscope slides using a 9mm diameter, 120µm thick adhesive imaging gasket (Grace BioLabs, OR, USA) filled with water.

2.3 Spontaneous Raman imaging

Spontaneous Raman spectra were acquired using a confocal micro-spectroscopy set-up, specifically, a Ti-U microscope stand with a 40x, 0.95NA objective and a 0.72NA condenser. The 532nm laser excitation was filtered using a Semrock LL01-532 filter and coupled into the microscope by a dichroic mirror (Semrock LPD01-532RS). Raman scattering was collected in epi-direction, filtered with a long pass filter (Semrock BLP01-523R), dispersed by an imaging spectrometer (Horiba iHR550) with a grating of 300 lines/mm, and detected with a CCD camera (Andor Newton DU971N-BV). All measurements were performed at room temperature.

2.4 CARS microscope setup

Hyperspectral CARS imaging was performed using a home-built CARS setup[12]. A single Ti:Sa 5 fs broadband (660-970nm) laser provided the pump and Stokes components for the CARS excitation. The broadband laser output was spectrally separated by dichroic beam splitters, resulting in a pump beam with a centre wavelength at 682nm and a

Downloaded From: https://www.spiedigitallibrary.org/conference-proceedings-of-spie on 13 Mar 2019
Terms of Use: https://www.spiedigitallibrary.org/terms-of-use

bandwidth of 65nm, and a Stokes beam with a centre wavelength at 806nm and a bandwidth of 200nm. A spectral resolution of 10cm^{-1} was achieved through spectral focussing[33]. CARS spectroscopy over the 1200-3800cm^{-1} range was performed by changing the relative delay time between pump and Stokes pulses. The excitation beams were coupled into a commercial microscope stand (Nikon Ti-U) via a home-built scanning head. For all work presented here, a 60x, 1.27NA objective was used with a 1.4NA oil condenser, and the CARS signal was detected by a photomultiplier tube (Hamamatsu H7422-40). The microscope stand was also equipped with differential interference contrast (DIC) optics, which were utilised for selection of regions of interest within samples prior to CARS imaging. Hyperspectral CARS datasets were obtained by acquiring spatial images at different wavenumbers across the silent region of the Raman spectrum with a spectral step size of 5cm^{-1}. The 1800-2700cm^{-1} spectral range was targeted through use of a Semrock FF01-593/40 single-band bandpass filter, which we refer to as our "intermediate" filter, and a pixel dwell time of 0.1ms was used. For correct quantification of CARS intensity ratios, backgrounds were measured under the same excitation and detection conditions with pump and Stokes pulses out of time overlap (1000cm^{-1}) and were subtracted from the measured CARS intensities prior to data analysis.

2.5 Data analysis

Hyperspectral CARS images were initially noise-filtered with a singular value decomposition (SVD) algorithm on the square root of the CARS intensity to retain only components above noise[15]. CARS intensity ratios were then calculated by dividing the background-corrected CARS intensity by the corresponding non-resonant CARS intensity measured in glass under the same excitation and detection conditions. The phase-corrected Kramers-Kronig method (PCKK) was then used to retrieve from the CARS intensity ratio the complex CARS third-order susceptibility (normalised to the non-resonant value in glass), which is linear in the concentration of chemical components. Non-negative matrix factorisation applied to the imaginary part and the average real part of the susceptibility with an additional concentration constraint (FSC^3 method) was used to obtain susceptibility spectra of independently varying chemical components and their volume concentrations. The FSC^3 is unsupervised and thus does not require prior knowledge of the spectra of chemical components and instead uses random initial guesses. A detailed overview of the data analysis procedure is described in ref 15.

3. RESULTS & DISCUSSION

3.1 Raman characterisation of deuterated and non-deuterated oleic acid

Lipids can be imaged by CARS microscopy with high contrast due to their repeating chains of carbon and hydrogen and thus, CARS has become recognised as an effective method for imaging lipid droplets in a label-free manner[11,34,35,36], avoiding associated difficulties with labelling artefacts such as artificial induction of cytosolic lipid droplet fusion, which is frequently observed during standard staining protocols[37,38,39]. When cells are exposed to high concentrations of lipid, the excess lipid is stored in dense, spherical droplets, which present excellent imaging targets for CARS due to the high localisation of carbon-hydrogen bonds. Due to these favourable properties, we have utilised deuterated lipid in a proof-of-concept study to assess the capability of our in-house-built multimodal CARS microscope setup for imaging molecules labelled through selective replacement of hydrogen atoms with deuterium. In addition to the superior CARS sensitivity offered by lipid droplets, they also provide a clear focal point for imaging following exogenous application of a deuterated fatty acid, i.e. we already know the precise location where our deuterated molecule will accumulate following cellular uptake. Our in-house built CARS system features three separate bandpass filters, specifically set up for imaging each of the three characteristic regions of the Raman spectra, and we have utilised our "intermediate" filter to image within the silent region of the Raman spectrum (1800-2700cm^{-1}), targeting the carbon-deuterium-associated peak at ~2100cm^{-1}.

We studied a deuterated isoform of oleic acid containing 17 carbon-deuterium bonds (D17-OA), as well as the non-deuterated form of the fatty acid (OA). Spontaneous Raman spectra were initially acquired for pure forms of D17-

Downloaded From: https://www.spiedigitallibrary.org/conference-proceedings-of-spie on 13 Mar 2019
Terms of Use: https://www.spiedigitallibrary.org/terms-of-use

OA and OA in liquid phase, enabling identification of carbon-deuterium-associated peak position and observation of differences between spectra for the deuterated and non-deuterated fatty acid. The Raman spectra shown in Figure 1 provide a reference for interpretation of CARS intensity spectra, in which molecular peaks are more difficult to assign due to interference between resonant and non-resonant terms of the susceptibility $\chi^{(3)}$. The attribution of each spectral peak to its associated chemical group is summarised in Table 2.

The fingerprint region exhibits well-characterised vibrational peaks[40,41] including a $\delta(CH_2)$ twist peak at approximately 1290cm^{-1}, and a $\delta(CH_2)/\delta(CH_3)$ deformation peak between 1400cm^{-1} and 1500cm^{-1}. For both fatty acid isoforms shown in Figure 1, the $\delta(CH_2)$ peak divides into two peaks at 1260cm^{-1} and 1300cm^{-1} attributed to δ(=CH) and $\delta(CH_2)$ deformations, respectively, due to unsaturation of the acyl chain, and the peak present at 1660cm^{-1} corresponds to v(C=C) stretch. Furthermore, the peaks at 1300cm^{-1} and 1400-1500cm^{-1} are reduced in the D17-OA spectrum due to fewer CH_2 and CH_3 groups present as a result of deuterium incorporation. Peaks within the CH-stretch region are more difficult to attribute due to a large degree of overlap between vibrational resonances. The peak at 2855cm^{-1} is attributed to CH_2 symmetric stretch; the peak at 2880cm^{-1} is attributed to a combination of CH_2 asymmetric stretch vibrations and Fermi resonance interactions with overtones originating from CH_2 and CH_3 deformations; and the peak at 2930cm^{-1} is generated by overlap between CH_3 stretch vibrations and CH_2 asymmetric stretch vibrations[29]. A reduced intensity is observed for both peaks within the D17-OA spectrum due to a reduced total number of carbon-hydrogen bonds as a result of deuterium incorporation. The peak at 3010cm^{-1} is attributed to v(=CH) stretch and does not change between the oleic acid isoforms. Incorporation of a deuterium atom induces a down-shift of the CH-associated peaks from the CH-stretch region into the silent region of the Raman spectrum. Thus, for D17-OA, a CD-associated peak is present at around 2100cm^{-1}. As is observed in the CH-stretch region, the CD-associated peaks show overlap of vibrational resonances, making assignment of peaks challenging. It should also be noted that the small peak at 2330cm^{-1} corresponds to nitrogen present within the glass of the microscope slide and coverslip and is not related to CD-associated resonances.

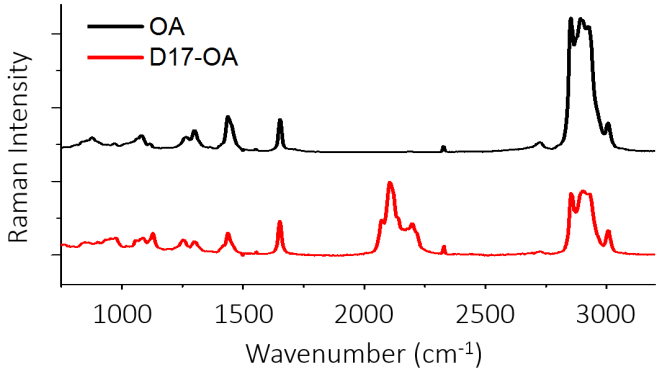

Figure 1. Spontaneous Raman spectra for deuterated and non-deuterated oleic acid. Spectra are vertically shifted in respect to each other for clarity. OA: oleic acid; D17-OA: D17-oleic acid.

Downloaded From: https://www.spiedigitallibrary.org/conference-proceedings-of-spie on 13 Mar 2019
Terms of Use: https://www.spiedigitallibrary.org/terms-of-use

Table 2. Overview of Raman vibrational resonances for investigated lipids. Assignments are made for peaks from the fingerprint, silent and CH-stretch regions of the Raman spectrum.

Wavenumber (cm^{-1})	**Assignment**
1260	δ(=CH) deformation
1290	$\delta(CH_2)$ twist
1300	$\delta(CH_2)$ deformation
1400-1500	$\delta(CH_2)/\delta(CH_3)$ deformation
1660	v(C=C) stretch
2070-2200	CD-associated resonances
2855	CH_2 symmetric stretch
2880	CH_2 asymmetric stretch and Fermi resonance interactions with overtones originating from CH_2 and CH_3 deformations
2930	CH_3 stretch and CH_2 asymmetric stretch
3010	v(=CH) stretch

3.2 Identification of intracellular deuterated lipid

To assess the capability of our in-house-built multimodal CARS system for identifying and spatially resolving a deuterium-labelled molecule within a cell, HeLa cells were treated with D17-OA and their lipid droplets were imaged by hyperspectral CARS, specifically targeting the silent region of the Raman spectrum (1800-2700cm^{-1}) where the C-D resonance is situated (~2100cm^{-1}). Subsequent data processing enabled production of spatially resolved, chemically specific images. HeLa cells were initially incubated in lipid-free serum-containing growth media for 18 hours to deplete lipid stores, before being treated with either D17-OA or OA for a further 18 hours, over which time the exogenously applied lipids were accumulated in lipid droplets. Hyperspectral CARS datasets were obtained by acquiring XY images at a series of wavenumbers to give a spectrum for each pixel of the spatial image. Post-acquisition processing of the hyperspectral CARS data was then performed to produce Raman-like spectra, which were linear in concentration of chemical components and compatible with our factorisation into susceptibilities and concentrations of chemical components (FSC^3) algorithm, which could then be used to identify independent chemical components and their volume concentrations in an unsupervised manner (see ref. 15 for detailed description). Here we use FSC^3 analysis to directly compare chemical components of D17-OA- and non-deuterated OA-treated cells.

Figure 2 shows the outputs of the unsupervised FSC^3 analysis for HeLa cells treated with D17-OA and non-deuterated OA. The main spectral components of the XY images are identified and displayed as spatial concentration maps. Four separate chemical components were considered in the factorisation algorithm, which was the minimum number required to well-represent the lipid composition of the droplets within the field of view. DIC images were acquired for initial visualisation of whole cells and selection of regions for hyperspectral CARS imaging. Based on the localisation of signal within the spatially resolved images as well as the lack of observable peaks present in the retrieved spectrum over the measured wavenumber range, Component 1 is considered to represent the aqueous medium

Downloaded From: https://www.spiedigitallibrary.org/conference-proceedings-of-spie on 13 Mar 2019
Terms of Use: https://www.spiedigitallibrary.org/terms-of-use

surrounding the lipid droplets, primarily water. Similarly, Component 2 shows no distinguishable peaks within its retrieved spectrum and is thus considered to represent a mixed signal predominated by water. Component 3 can be attributed to D17-OA as its signal is localised within lipid droplets and a prominent peak is observed within its retrieved spectrum at approximately 2100cm^{-1}, corresponding to C-D bond vibration. Lipid droplets showing a D17-OA signal are only visible in the spatially resolved images acquired from the D17-OA-treated HeLa cells and are completely absent from cells fed with non-deuterated OA. A peak at around 2850cm^{-1} is also observed in the retrieved spectrum for Component 3, which corresponds to C-H bond vibrations. This peak arises as D17-OA is not fully deuterated and a portion of the aliphatic chain still contains C-H bonds. This peak is also present in the retrieved spectrum for Component 4 but at a higher intensity, thus this component can be attributed to non-deuterated OA based on the absence of a peak at ~2100cm^{-1} and the localisation of signal to lipid droplets. Although some signal is present within lipid droplets of D17-OA-treated cells for Component 4 due to the presence of some C-H bonds, the observed spatially resolved signal and peak intensity are comparably larger in cells treated with OA due to a larger total number of C-H bonds.

These results display the capability of our in-house-built multimodal CARS imaging setup and subsequent data processing methods to identify and distinguish a deuterated fatty acid component from the complex chemical background of a cell with a high spatial resolution and quantitative chemical specificity.

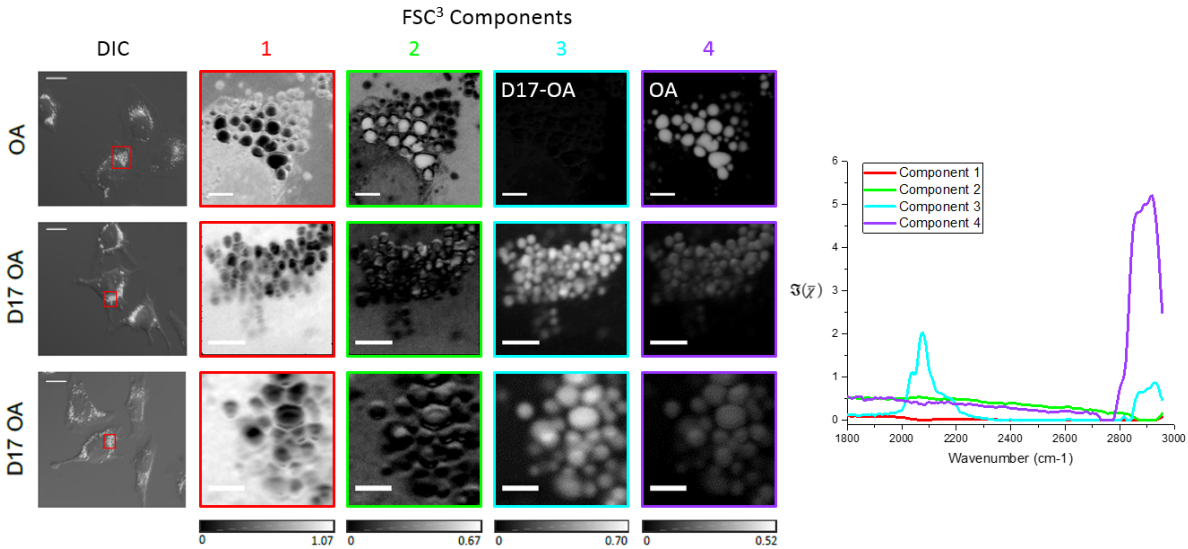

Figure 2. Spatial and spectral outputs from unsupervised FSC^3 analysis of hyperspectral CARS datasets for OA- and D17-OA-treated HeLa cells, specifically targeted within the silent region of the Raman spectrum. The concentration maps identify and spatially resolve four components which are chemically specified by their representative spectra showing the phase-retrieved imaginary part of the normalised CARS susceptibility $\Im(\bar{\chi})$. Components are identified corresponding to (primarily) water (Components 1 and 2), D17-OA (Component 3), and non-deuterated OA (Component 4). Volume concentration ranges are shown on a grayscale. DIC images show whole cells and the lipid-rich regions selected for hyperspectral CARS acquisition. Scale bars show 20µm in DIC images and 4µm in FSC^3 images (except for lowest row which shows 2µm).

3.3 Cross-modality conservation of C-D peak shape

Figure 3 shows direct comparison between CARS spectra retrieved from a pure droplet of D17-OA in liquid phase and from intracellular lipid droplets within HeLa cells. The previously shown spontaneous Raman spectrum for pure D17-OA is also included for reference. The line-shape of the C-D-associated peak at ~2100cm^{-1} is well-conserved

Downloaded From: https://www.spiedigitallibrary.org/conference-proceedings-of-spie on 13 Mar 2019
Terms of Use: https://www.spiedigitallibrary.org/terms-of-use

across the three spectra, illustrating the precision with which our FSC^3 data processing procedure can identify a chemical component corresponding to a deuterium-labelled molecule within a cell sample. Through use of our "intermediate" bandpass filter, we are able to specifically target the silent region of the Raman spectrum (1800-2700cm^{-1}) and achieve a large signal above noise for C-D-associated vibrations within this spectral range. Changes in line-shape are, however, observed for the C-H peak at ~2850cm^{-1} across the three spectra due to an upper limit of the intermediate filter at ~3000cm^{-1}. The observed line-shape for peaks situated close to this upper limit can appear altered, and therefore, for measurements where expected peaks are located above ~2800cm^{-1}, we use our C-H-targeted bandpass filter (Semrock FF01-562/40).

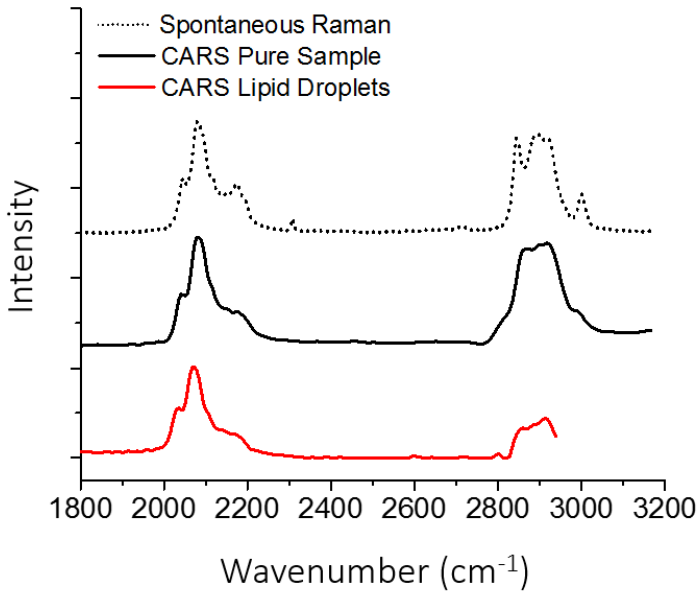

Figure 3. Comparison of spectral line-shapes within the silent region of the Raman spectrum, specifically showing conservation of C-D peak-shape across techniques. Retrieved CARS spectra acquired from pure D17-OA and lipid droplets of a D17-OA-treated HeLa cell were compared with the spontaneous Raman spectrum for D17-OA. Spectra are vertically shifted in respect to each other for clarity.

4. CONCLUSION AND OUTLOOK

We have described the ability of our in-house-developed multimodal CARS imaging system and subsequent data processing pipeline to identify and spatially resolve a chemical component corresponding to a deuterium-labelled molecule, specifically D17-OA, within a cell. Our FSC^3 algorithm provides us with high-resolution concentration maps, as well as retrieved CARS spectra which permit chemical specificity with a high degree of accuracy. In principle, we have used a deuterated isoform of oleic acid to illustrate that our CARS system can be used to observe the intracellular localisation of an exogenously applied, deuterium-labelled molecule.

These results indicate potential for further application of this strategy, where deuterium can be incorporated into a variety of other molecules which are poorly suited to fluorescence imaging. These molecules can then be imaged using our in-house CARS system for assessment of localisation and metabolism. Furthermore, there is demand within the pharmaceutical industry for assessing intracellular distribution, accumulation and turnover of small molecules which

Downloaded From: https://www.spiedigitallibrary.org/conference-proceedings-of-spie on 13 Mar 2019
Terms of Use: https://www.spiedigitallibrary.org/terms-of-use

cannot be labelled with fluorescent markers. Due to the minimal structural change induced with deuterium incorporation, its combination with CARS microscopy may provide a means by which this can be achieved.

The main challenge we face is achieving sufficient signal above noise to observe a deuterated molecule of interest against the complex chemical background of the cell. Even though our data processing procedure helps us to maximise the observed signal from C-D bond vibrations, there is still a requirement for the molecule of interest to accumulate within a concentrated area if contrast is to be achieved. We have described the high signal-to-noise ratio within the silent region of the Raman spectrum shown by D17-OA, largely due to accumulation within highly concentrated droplets, which enabled a D17-OA component to be clearly identified and spatially resolved by our FSC^3 algorithm. However, if a molecule does not accumulate as readily within a given area of the cell, our CARS system may struggle to identify and distinguish it from the chemical background, presenting a challenge in future studies where we aim to visualise molecules with a less localised intracellular distribution.

5. ACKNOWLEDGMENTS

DB, SH and PW would like to acknowledge support from GlaxoSmithKline and the UK BBSRC Research Council (BB/N50371X/1). PB acknowledges the Royal Society for her Wolfson Research Merit award (WM140077).

REFERENCES

[1] Watson, P., Jones, A. T. & Stephens, D. J. Intracellular trafficking pathways and drug delivery: fluorescence imaging of living and fixed cells, Adv Drug Deliv Rev 57, 43-61 (2005)

[2] Theillet, F., Binolfi, A., Frembgen-Kesner, T., Hingorani, K., Sarkar, M., Kyne, C., Li, C., Crowley, P. B., Gierasch, L., Pielak, G. J., Elcock, A. H., Gershenson, A. & Selenko, P. Physicochemical properties of cells and their effects on intrinsically disordered proteins (IDPs), Chem Rev 114, 6661 (2014)

[3] Yin, L., Wang, W., Wang, S., Zhang, F., Zhang, S. & Tao, N. How does fluorescent labelling affect the binding kinetics of proteins with intact cells? Biosens Bioelectron 66, 412-416 (2015)

[4] Hann, M. M., Leach, A. R. & Harper, G. Molecular complexity and its impact on the probability of finding leads for drug discovery, J Chem Inf Comput Sci 41, 856-864 (2001)

[5] Bemis, G. W. & Murcko, M. A. The properties of known drugs. 1. Molecular Frameworks, J Med Chem 39, 2887-2893 (1996)

[6] Hoebe, R. A., Van Oven, C. H., Gadella Jr, T. W. J., Dhonukshe, P. B., Van Noorden, C. J. F. & Manders E. M. M. Controlled light-exposure microscopy reduces photobleaching and phototoxicity in fluorescence live-cell imaging, Nature Biotechnology 25, 249-253 (2007)

[7] Pope, I., Langbein, W., Borri, P. & Watson, P. Live cell imaging with chemical specificity using dual frequency CARS microscopy. In: Conn, PM ed., Imaging and spectroscopic analysis of living cells: Optical and spectroscopic techniques, Methods in Enzymology 504, 273-291 (2012)

[8] Smith, R., Wright, K. L. & Ashton, L. Raman spectroscopy: An evolving technique for live cell studies, Analyst 141, 3590-3600 (2016)

[9] Sijtsema, N. M., Wouters, S. D., de Grauw, C. J., Otto, C. & Greve, J. Confocal direct imaging Raman microscope: Design and applications in biology, Applied Spectroscopy 52, 348-355 (1998)

[10] Zumbusch, A., Holtom, G. R. & Xie, X. S. Three-dimensional vibrational imaging by coherent anti-Stokes Raman scattering, Physical Review Letters 82, 4142 (1999)

Downloaded From: https://www.spiedigitallibrary.org/conference-proceedings-of-spie on 13 Mar 2019
Terms of Use: https://www.spiedigitallibrary.org/terms-of-use

[11] Zumbusch, A., Langbein, W. & Borri, P. Nonlinear vibrational microscopy applied to lipid biology, Progress in Lipid Research 52, 615-632 (2013)
[12] Pope, I., Langbein, W., Watson, P. & Borri, P. Simultaneous hyperspectral differential-CARS, TPF and SHG mictoscopy with a single 5 fs Ti:Sa laser, Optics Express 21, 7096-7106 (2013)
[13] Vartianen, E. M., Rinia, H. A., Müller, M. & Bonn, M. Direct extraction of Raman line-shapes from congested CARS spectra, Optics Express 14, 3622-3630 (2006)
[14] Liu, Y., Lee, Y. J. & Cicerone, M. T. Broadband CARS spectral phase retrieval using a time-domain Kramers-Kronig transform, Optics Letters 34, 1363-1365 (2009)
[15] Masia, F., Glen, A., Stephens, P., Borri, P. & Langbein, W. Quantitative chemical imaging and unsupervised analysis using hyperspectral coherent anti-Stokes Raman scattering microscopy, Anal Chem 85, 10820-10828 (2013)
[16] Chung, C. Y., Boik, J. & Potma, E. O. Biomolecular imaging with coherent nonlinear vibrational microscopy, Annu Rev Phys Chem 64, 77-99 (2013)
[17] Tipping, W. J., Lee, M., Serrels, A., Brunton, V. G. & Hulme, A. N. Stimulated Raman scattering microscopy: an emerging tool for drug discovery, Chem Soc Rev 45, 2075-2089 (2016)
[18] Nan, X., Yang, Y. & Xie, X. S. CARS microscopy: Lights up lipids in living cells, Biophotonics International 11, 44 (2004)
[19] Bergner, G., Chatzipapadopoulos, S., Akimov, D., Dietzek, B., Malsch, D., Henkel, T., Schlücker, S. & Popp, J. Quantitative CARS microscopic detection of analytes and their isotopomers in a two-channel microfluidic chip, Small 5, 2816-2818 (2009)
[20] Bergner, G., Albert, C. R., Schiller, M., Bringmann, G., Schirmeister, T., Dietzek, B., Niebling, S., Schlücker, S., & Popp, J. Quantitative detection of C-deuterated drugs by CARS microscopy and Raman microspectroscopy, Analyst 136, 3686-3693 (2011)
[21] Stiebing, C., Matthäus, C., Krafft, C., Keller, A. A., Weber, K., Lorkowski, S. & Popp, J. Complexity of fatty acid distribution inside human macrophages on single cell level using Raman micro-spectroscopy, Anal Bioanal Chem 406, 7037-7046 (2014)
[22] Matthäus, C., Krafft, C., Dietzek, B., Brehm, B. R., Lorkowski, S. & Popp, J. Noninvasive imaging of intracellular lipid metabolism in macrophages by Raman microscopy in combination with stable isotopic labelling, Anal Chem 84, 8549-8556 (2012)
[23] Alfonso-Garcia, A., Pfisterer, S. G., Riezman, H., Ikonen, E. & Potma, E. O. D38-cholestrol as a Raman active probe for imaging intracellular cholesterol storage, Journal of Biomedical Optics 21, 061003 (2016)
[24] Lee, H. J. & Cheng, J. Imaging chemistry inside living cells by stimulated Raman scattering microscopy, Methods 128, 119-128 (2017)
[25] Wei, L., Yu, Y., Shen, Y., Wang, M. C. & Min, W. Vibrational imaging of newly synthesised proteins in live cells by stimulated Raman scattering microscopy, Proc Natl Acad Sci USA 110, 11226-11231 (2013)
[26] Wei, L., Shen, Y., Xu, F., Hu, F., Harrington, J. K., Targoff, K. L., Min, W. Imaging complex protein metabolism in live organisms by stimulated Raman scattering microscopy with isotope labelling, ACS Chem Biol 10, 901-908 (2015)
[27] Stiebing, C., Meyer, T., Rimke, I., Matthäus, C., Schmitt, M., Lorkowski, S. & Popp, J. Real-time Raman and SRA imaging of living human macrophages reveals cell-to-cell heterogeneity and dynamics of lipid uptake, J Biophotonics 10, 1217-1226 (2017)
[28] Li, J. & Cheng, J. Direct visualisation of de novo lipogenesis in single living cells, Sci Rep 4, 6807 (2014)
[29] Di Napoli, C., Masia, F., Pope, I., Otto, C., Langbein, W. & Borri, P. Chemically-specific dual/differential CARS micro-spectroscopy of saturated and unsaturated lipid droplets, J Biophotonics 7, 68-76 (2014)
[30] Di Napoli, C., Pope, I., Masia, F., Watson, P., Langbein, W. & Borri, P. Hyperspectral and differential CARS microscopy for quantitative chemical imaging in human adipocytes, Biomed Opt Express 5, 1378-1390 (2014)

Downloaded From: https://www.spiedigitallibrary.org/conference-proceedings-of-spie on 13 Mar 2019
Terms of Use: https://www.spiedigitallibrary.org/terms-of-use

[31] Di Napoli, C., Pope, I., Masia, F., Langbein, W., Watson, P. & Borri, P. Quantitative spatiotemporal chemical profiling of individual lipid droplets by hyperspectral CARS microscopy in living human adipose-derived stem cells, Anal Chem 88, 3677-3685 (2016)
[32] Listenberger, L.L. & Brown, D. A. Fluorescent detection of lipid droplets and associated proteins, Current Protocols in Cell Biology, 24.2.1-24.2.11 (2007)
[33] Rocha-Mendoza, I., Langbein, W., Borri, P. Coherent anti-Stokes Raman microspectroscopy using spectral focussing with glass dispersion, Appl Phys Lett 93, 201103 (2008)
[34] Evans, C. L. & Xie, X. S. Coherent anti-Stokes Raman scattering microscopy: chemical imaging for biology and medicine, Annu Rev Anal Chem 1, 883-909 (2008)
[35] Rinia, H. A., Burger, K. N. J., Bonn, M. & Müller, M. Quantitative label-free imaging of lipid composition and packing of individual cellular lipid droplets using multiplex CARS microscopy, Biophysical Journal 95, 4908-4914 (2008)
[36] Paar, M., Jüngst, C., Steiner, N. A., Magnes, C., Sinner, F., Kolb, D., Lass, A., Zimmermann, R., Zumbusch, A., Kohlwein, S. D. & Wolinski, H. Remodeling of lipid droplets during lipolysis and growth in adipocytes, J Biol Chem 287, 11164-11173 (2012)
[37] Fukumoto, S. & Fujimoto, T. Deformation of lipid droplets in fixed samples, Histochem Cell Biol 118, 423-428 (2002)
[38] Nan, X., Cheng, J. X. & Xie, X. S. Vibrational imaging of lipid droplets in live fibroblast cells with coherent anti-Stokes Raman scattering microscopy, J Lipid Res 44, 2202-2208 (2003)
[39] Ohsaki, Y., Shinohara, Y., Suzuki, M. & Fujimoto, T. A pitfall in using bodipy dyes to label lipid droplets for fluorescence microscopy, Histochem Cell Biol 133, 477-480 (2010)
[40] De Gelder, J., De Gussem, K., Vandenabeele, P. & Moens, L. Reference database of Raman spectra of biological molecules. J Raman Spectrosc 38, 1133-1147 (2007)
[41] Verma, S. P. & Wallach, D. F. H. Raman spectra of some saturated, unsaturated and deuterated C_{18} fatty acids in the HCH-deformation and CH-stretching regions. Biochimica et Biophysica Acta 486, 217-227 (1977)

Downloaded From: https://www.spiedigitallibrary.org/conference-proceedings-of-spie on 13 Mar 2019
Terms of Use: https://www.spiedigitallibrary.org/terms-of-use